Simplified Two-Fluid Model for Gas-Lift Efficiency Predictions

S. Guet and G. Ooms
J.M. Burgerscentrum, Laboratory for Aero- and Hydrodynamics, Delft University of Technology, 2628 CA Delft, The Netherlands

R. V. A. Oliemans
J.M. Burgerscentrum, Kramers Laboratorium, Delft University of Technology, 2628 BW Delft, The Netherlands

DOI 10.1002/aic.10444
Published online April 28, 2005 in Wiley InterScience (www.interscience.wiley.com).

A simplified Euler–Euler model was developed for predicting the void fraction and velocity profiles in a vertical upward bubbly pipe flow. The main objective of this approach is to provide a tool for computing the gravitational pressure gradient associated with a large number of flow conditions. This model is based on existing correlations for the interfacial momentum transfer and turbulence modeling. Assuming a fully developed, axially symmetric flow, our formulation reduces to a set of first-order equations, which can be solved with relatively fast convergence. The results obtained with our approach are first validated by comparisons with experiments collected in small-diameter tubes taken from the literature. Then, the model results are compared with our experiments at low liquid input, moderate pipe diameter conditions and for various bubble size values. The model is found to correctly predict the evolution of void fraction and velocity profiles associated with bubble size and liquid input changes. The drift-flux model distribution parameter and the superficial gas velocity for various flow conditions was finally computed. The results show a reasonable comparison with experiments. © 2005 American Institute of Chemical Engineers *AIChE J,* 51: 1885–1896, 2005
Keywords: bubbly flow, pipe, two-fluid model, gas lift

Introduction

Modeling the relevant physical phenomena for predicting the phase and velocity radial distributions in upward bubbly pipe flows is a challenging issue. The main difficulties are associated with the dependency of the void fraction radial profile on the bubble size and flow conditions, and the coupling between the void fraction and velocity profiles. To solve this problem, the two-fluid or Euler–Euler modeling approach (Ishii, 1975) is often applied for vertical upward bubbly pipe flow predictions (Chahed and Masbernat, 1998; Drew and Lahey, 1982; Hill et al., 1995; Lopez de Bertodano, 1994; Lucas et al., 2001; Politano et al., 2003). In this modeling method, also called two-fluid model, both the continuous phase and the dispersed phase are considered as a continuum. The mass and momentum conservation equations are averaged and given in Eulerian coordinates.

The aim of the present contribution is to develop a simplified model able to predict the main effects of bubble size and liquid input on the gravitational pressure gradient in vertical upward bubbly pipe flows. We want to develop a fast converging Euler–Euler model able to capture the main changes of void fraction and liquid velocity radial profiles attributed to bubble size and liquid input effects, based on available models for the interfacial momentum transfer and turbulence modeling. If validated, such a model will ultimately enable to study the

Correspondence concerning this article should be addressed to S. Guet at sebastien.guet@ifp.fr.

effect of various combinations of bubble size and liquid input conditions on the gravitational pressure gradient.

The bubble size is known to affect the void fraction transverse profiles in vertical pipe flows. Small bubbles accumulate at the wall to form a wall-peaking radial distribution, whereas large bubbles migrate to the centerline zone of the pipe and lead to a core-peaking void fraction distribution. Recently, it was shown that the evolution of the transverse void fraction profile with increased bubble size could be properly described by using an appropriate model for the lift force, as proposed in Tomiyama (1998) and Tomiyama et al. (2002) (Lucas et al., 2001; Politano et al., 2003). In this model, the lift-force coefficient changes sign with increased bubble diameter as a result of the effects of bubble deformation on the bubble wake–shear field interactions. In addition, a lubrication type of repulsion force at the near wall, as suggested in Antal et al. (1991), brought significant improvements for proper near-wall void fraction predictions. Because the lift force is proportional to the radial gradient of the axial component of liquid velocity in vertical bubbly pipe flow, a strong coupling between the void fraction and the liquid velocity radial profiles can be expected.

Also the liquid input conditions influence the transverse profiles of both liquid velocity and void fraction. At low enough liquid input, a downflow of liquid at the wall can be observed, similar to that in bubble column flows (Mudde and Saito, 2001; Mudde et al., 1997). This in turn can be expected to affect the void fraction profile: the liquid velocity gradient changes sign near the wall, which might result in an inversed lift-force direction in that area. Therefore, to determine the void fraction profile at low liquid input conditions, both the bubble size and the effects due to the liquid velocity profile are important.

The gas-lift technique is a gravity-driven pumping technique, which uses gas injection to reduce the gravitational pressure in vertical oil wells. The reduced pressure compared to that of single-phase liquid flow either generates or increases the liquid input. To quantify the gas-lift efficiency changes stemming from the effects of bubble size and liquid input, we will compute the distribution parameter C_0 of the drift-flux model (Zuber and Findlay, 1965) for various flow conditions. This parameter C_0 directly connects the area average void fraction to the superficial gas and liquid velocities by

$$\frac{U_{sg}}{\langle \varepsilon \rangle} = C_0(U_{sg} + U_{sl}) + |U_{drift}| \tag{1}$$

in which $|U_{drift}|$ is the weighted mean drift velocity defined by

$$|U_{drift}| = \frac{\int_A \varepsilon U_{drift} dA}{\int_A \varepsilon dA} \tag{2}$$

The distribution parameter C_0 is given by

$$C_0 = A \frac{\int_A \varepsilon j dA}{\int_A \varepsilon dA \int_A j dA} \tag{3}$$

where ε is the void fraction, A is the pipe cross section, and j is the (local) mixture flux: $j = \varepsilon U_g + (1 - \varepsilon)U_l$. The gas drift velocity U_{drift} is defined as $U_{drift} = U_g - j$. It is clear from Eq. 1, that provided $|U_{drift}|$ is known the distribution parameter C_0 given by Eq. 3 can be used to quantify the gravitational pressure gradient for given gas and liquid superficial velocities U_{sg} and U_{sl}. Such a result permits an evaluation of the gas-lift efficiency when operating at low liquid input because in those conditions the frictional pressure drop is negligible with respect to the gravitational contribution (Guet et al., 2003a).

In a previous study, we measured the radial profiles of void fraction and phase velocities associated with various bubble size and liquid input conditions in a 72-mm inner-diameter pipe flow experimental setup (Guet et al., 2004). The measurement techniques used for that purpose were a four-point optical fiber probe for the bubble velocity and size determination (Guet et al., 2003b; Mudde and Saito, 2001), and laser Doppler anemometry for the liquid-phase velocity characterization (Guet et al., 2002). Based on these measurements, we computed the distribution parameter C_0 by applying Eq. 3 to the measured profiles of void fraction and velocities. Because of the changes in the void fraction and velocity distributions, significant variations of the drift-flux model distribution parameter were found when varying the bubble size and the liquid input conditions, from $C_0 \approx 0.95$ for large liquid input flow with small bubbles to $C_0 \approx 1.5$ for low liquid input conditions with large bubbles (Guet et al., 2004).

The changes of the C_0 parameter will be investigated with a numerical model in the present study. The advantage of developing such a model is its potential ability to upscale our experimental results to different pipe diameter and fluid properties. Our predictions for the void fraction and velocity profiles will be first compared with experiments reported by Liu and Bankoff (1993) and Serizawa et al. (1975) for pipe diameters $D_p = 38$ and 60 mm, respectively. Then, the model results will be compared with our experimental data collected on a 72-mm-diameter pipe flow experimental setup. Various liquid input and bubble size conditions will be compared. Finally, the distribution parameter C_0 of the drift-flux model will be computed for a large range of liquid input and bubble size conditions, and compared with our set of experimental data.

Model Formulation

Averaged equations

The phase indicator functions X_k, where $k = g$ or l for the gas and the liquid phase, respectively, are introduced

$$X_k(\vec{x}, t) = \begin{cases} 1 & \text{if } \vec{x} \text{ is in phase } k \\ 0 & \text{otherwise} \end{cases}$$

The phase indicators X_k are advected by phase k

$$\frac{\partial X_k}{\partial t} + \vec{u}_k \cdot \vec{\nabla}(X_k) = 0 \tag{4}$$

and the averaged value of the phase indicator leads to the k-phase–averaged fraction

$$\varepsilon_k = \langle X_k \rangle \tag{5}$$

The velocity is decomposed into an average and a fluctuating part $\vec{u}_k = \vec{U}_k + \vec{u}'_k$, with $\vec{U}_k = \langle \vec{u}_k \rangle$. After averaging the continuity and momentum conservation equation for the gas and the liquid phases, the following set of equations is obtained ($k = g$ or l)

$$\frac{\partial(\varepsilon_k \rho_k)}{\partial t} + \vec{\nabla} \cdot (\varepsilon_k \rho_k \vec{U}_k) = 0 \tag{6}$$

$$\frac{\partial(\varepsilon_k \rho_k \vec{U}_k)}{\partial t} + \vec{\nabla} \cdot (\varepsilon_k \rho_k \vec{U}_k \vec{U}_k^t) = \varepsilon_k \rho_k \vec{g} + \varepsilon_k \vec{\nabla} \cdot (\tau_{kT}) - \varepsilon_k \vec{\nabla} P_k + \vec{M}_k + (\tau_{kT} - \tau_{kI}) \vec{\nabla} \varepsilon \tag{7}$$

where ρ_k, U_k, Pk, and ε_k are, respectively, the average density, velocity, pressure, and the volume fraction of phase k. $\vec{M}_k$ is the interfacial momentum transfer, τ_{kT} denotes the average total stress tensor, and τ_{kI} is the average total stress tensor at the interface. The total stress constitutes a viscous shear and a turbulence part

$$\tau_{kT} = \tau_k^{\mu} + \tau_k^{\mathrm{Re}} \tag{8}$$

where τ_k^{μ} is the viscous contribution and τ_k^{Re} is the Reynolds stress tensor representing the contribution arising from turbulence.

Interfacial Momentum Transfer

The interfacial momentum transfer is decomposed into

$$\vec{M}_k = (P_{kI} - P_k) \vec{\nabla} \varepsilon_k + \vec{F}_k \tag{9}$$

where the first term on the right-hand side denotes the interfacial pressure density. It takes into account the effect of the average interfacial pressure P_{kI}, different from the far-field pressure P_k. The second term $\vec{F}_k$ represents all the other interfacial forces. The interfacial force $\vec{F}_k$ is expressed as follows

$$\vec{F}_k = \vec{F}_{k,drag} + \vec{F}_{k,lift} + \vec{F}_{k,wall} + \vec{F}_{k,td} \tag{10}$$

where $\vec{F}_{k,drag}$ is the drag force, $\vec{F}_{k,lift}$ is the lift force, $\vec{F}_{k,wall}$ is a wall force, and $\vec{F}_{k,td}$ is a turbulent dispersion force, which can be included in different ways. By considering no mass transfer between phases and neglecting surface tension forces, we will assume $\vec{F}_g = -\vec{F}_l$.

A Simple Two-Fluid Model for Vertical Bubbly Pipe Flow

Assumptions

A simple version of the two-fluid model is formulated. The assumptions are the following:

(1) The flow is stationary ($\partial/\partial t = 0$).

(2) The flow is fully developed [$\partial U_k/\partial z = 0$ and $\partial \varepsilon_k/\partial z = 0$]. Although bubbles will always expand and/or coalesce, far from the entrance boundaries this hypothesis is locally valid.

(3) In the gas phase, both the gravity and stress terms are neglected because of the low density and viscosity.

(4) In the liquid phase, the difference between the average stress tensor and the interfacial stress tensor is neglected.

(5) The relative velocity $U_r = |\vec{U}_b - \vec{U}_l|$ between the gas and the liquid phase is constant in the radial direction. This assumption is an important simplification of the problem because, in general, we observed with our experiments that the bubble relative velocity decreases with increasing void fraction; however, the bubble slip velocity radial changes were small in comparison to the radial heterogeneities of void fraction and of phase velocity (Guet et al., 2004). The bubble relative velocity changes with the radial position are typically of $\pm 30\%$ magnitude, whereas the void fraction and the phase velocity can vary by $\pm 500\%$ in the radial direction. Also, the results will show that the most relevant effects arise from the lift force, and thus the radial changes of liquid velocity are the most relevant (the lift force is proportional to the liquid velocity gradient). In addition, it was previously shown that the mean bubble relative velocity could properly be described by using correlations based on the area-average void fraction (Guet et al., 2004). For these reasons, the bubble relative velocity is considered as constant in the radial direction in our simplified model.

Closure formulation

Drag Force. The drag force density is given by

$$\vec{F}_{g,drag} = -\frac{3}{8} \frac{\varepsilon}{R_b} C_d \rho_l (\vec{U}_g - \vec{U}_l) |\vec{U}_g - \vec{U}_l| \tag{11}$$

in which $\varepsilon = \varepsilon_g$ and where the drag coefficient is taken as (Ishii and Zuber, 1979)

$$C_d = \frac{8}{3} (1 - \varepsilon)^2 \tag{12}$$

It should be emphasized that this relation is valid for a large sphere in a free shear flow. There is thus a limitation in terms of both bubble size and void fraction: at some critical value of the void fraction, the flow is known to shift to slug flow (Guet et al., 2003a). This transition is also dependent on bubble size and corresponds to critical void fraction values of 0.3 to 0.1.

Lift Force. The general formulation of the lift force is

$$\vec{F}_{g,lift} = -C_l \varepsilon \rho_l (\vec{U}_g - \vec{U}_l) \times (\vec{\nabla} \times \vec{U}_l) \tag{13}$$

which, in the frame of a preferential direction, fully established cocurrent shear flow, reduces to

$$\vec{F}_{g,lift} = -C_l \varepsilon \rho_l |\vec{U}_g - \vec{U}_l| \frac{\partial U_l}{\partial r} \vec{e}_r \tag{14}$$

The lift coefficient is typically $C_l = 0.5$ for a single particle in shear flows. Values of $C_l = 0.05$–0.3 were reported to properly describe wall-peaking void fraction experiments in pipes with the Euler–Euler formulation (Antal et al., 1991; Lance and Lopez de Bertodano, 1994; Lopez de Bertodano, 1994). More recently, models for the lift coefficient dependency on the bubble shape were proposed from bubble-tracking experiments

(Tomiyama, 1998; Tomiyama et al., 2002). In those experiments the shape of the bubbles was found to affect the symmetry of the bubble wake, and its interaction with the shear field. This resulted in a negative equivalent lift-force coefficient for large bubbles. Lucas et al. (2001) showed, by using the model proposed by Tomiyama (1998) and Tomiyama et al. (2002) in a two-fluid model, that both the wall-peaking and the core-peaking radial void fraction distributions could be qualitatively described.

This model is given by

$$C_l = \begin{cases} \min[0.288 \tanh(0.121 R_e), f(E_{o_d})] & \text{for } E_{o_d} < 4 \\ f(E_{o_d}) & \text{for } 4 < E_{o_d} < 10.7 \\ -0.29 & \text{for } 10.7 < E_{o_d} \end{cases}$$

with $f(E_{o_d}) = 0.00105E_{o_d}^3 - 0.0159E_{o_d}^2 - 0.0204E_{o_d} + 0.474$.

The bubble lift-force coefficient is then dependent on the bubble Reynolds number $R_e = \rho_l U_r D_b/\mu_l$ for small bubbles. For larger bubbles (typically $D_b > 1$ mm, that is, $R_e > 10^2$ for air–water flows), the lift-force coefficient is essentially affected by the bubble shape through a modified Eötvös number given by

$$E_{o_d} = \frac{g(\rho_l - \rho_g) D_H^2}{\sigma} \tag{15}$$

where D_H is the maximum horizontal dimension of the bubble. This maximum horizontal dimension is computed using the correlation proposed by Wellek et al. (1966) for the ellipsoidal-bubble aspect ratio

$$D_H = D_b(1 + 0.163E_o^{0.757})^{1/3} \tag{16}$$

in which the Eötvös number is given by

$$E_o = \frac{g(\rho_l - \rho_g) D_b^2}{\sigma} \tag{17}$$

where σ is the gas–liquid surface tension and D_b is the volumetric spherical-equivalent bubble diameter.

Wall Force. A local wall force, which acts to drive the bubbles away from the wall, has been modeled by Antal et al. (1991), following a similarity with lubrication theory. This wall force is expressed as

$$\vec{F}_{g,wall} = -\frac{\varepsilon\rho_l|\vec{U}_g - \vec{U}_l|^2}{R_b}\left[C_{w1} + C_{w2}\left(\frac{R_b}{y_0}\right)\right]\vec{e}_r \tag{18}$$

where $C_{w1} = -0.06|\vec{U}_g - \vec{U}_l| - 0.104$, $C_{w2} = 0.147$, and $y_0 = R - r$ is the local distance from the wall. This force is valid only in the near-wall region, and should tend to zero when the distance from the wall increases. The wall-repulsion force is taken into account for $F_{g,wall} < 0$ that is, for $r > R + (C_{w2}R_b/C_{w1})$ (Tomiyama, 1998; Troshko and Hassan, 2002). This wall force provided significant improvements to a proper near-wall void fraction description: the void fraction is observed to decrease toward a zero-value at the wall (we also observed this void fraction decrease in our experiments), whereas two-fluid models based on the lift force only would predict a maximum void fraction value at the wall for small bubbles. It should be emphasized that the wall force model proposed by Antal et al. (1991) is, in principle, applicable to laminar bubbly flows. This wall-force expression, however, is often applied to turbulent bubbly flow as well, and successfully predicts a decreased void fraction in the near-wall region (Lopez de Bertodano, 1994; Politano et al., 2003; Troshko and Hassan, 2002). Recently, improved models have been proposed for turbulent conditions (Lucas et al., 2001; Tomiyama et al., 2002) and for taking into account the effects of bubble deformation (Moraga et al., 2004). Such models could be used to further improve our wall-force formulation.

Dispersion Force. The turbulence in the liquid has the tendency to redistribute heterogeneities of the phase fractions. To model this effect, a turbulence dispersion term is included in the model. Contrary to microscopic diffusion terms included in the mass conservation equation, this effect is taken into account by an additional turbulent dispersion force in the momentum conservation equation (Drew, 2001; Moraga et al., 2003). Following a diffusion approach, this force is modeled as (Carrica et al., 1999; Hill et al., 1995; Politano et al., 2003; Troshko and Hassan, 2002)

$$\vec{F}_{g,td} = -\frac{3}{8}\rho_l\nu_t\frac{C_d}{R_b}|\vec{U}_g - \vec{U}_l|\vec{\nabla}\varepsilon \tag{19}$$

In this formulation ν_t is the turbulent viscosity, taken from the model described in the next section. Only the radial heterogeneities of void fraction are considered in the present model. Because the turbulent dispersion force is parallel to the void fraction gradient, in our model the turbulent dispersion force will be present in the radial direction momentum equations

$$\vec{F}_{g,td} = -\frac{3}{8}\rho_l\nu_t\frac{C_d}{R_b}|\vec{U}_g - \vec{U}_l|\frac{\partial\varepsilon}{\partial r}\vec{e}_r \tag{20}$$

Interfacial pressure

The area-averaged interfacial pressures P_{Il} and P_{gI} need to be related to the spatial average of the pressure. Near the bubble surface, the liquid velocity is greater than the far-field velocity. This results in a pressure difference, approximated by a potential flow solution

$$P_{Il} - P_l = -C_p\rho_l(1 - \varepsilon)|\vec{U}_g - \vec{U}_l|^2 \tag{21}$$

In this expression the coefficient $C_p = 1/4$ is valid for spherical particles (Stuhmiller, 1977). For oblate spheroid bubbles, this coefficient can be up to 0.71 (Lance and Lopez de Bertodano, 1994), whereas the value $C_p = 1$ is used in Lopez de Bertodano (1994) and Politano et al. (2003), who considered large bubbles. In view of the lack of correlations for C_p, we will use the value $C_p = 1/4$ in the present model. In contrast from P_{Il}, the following hypothesis is valid for the gas phase because of its low density: $P_{gI} = P_g$.

Reynolds stress closure

The pipe flow Euler–Euler contributions reported in the literature often use the k–ε or Reynolds stress model (RSM) approach to model turbulence. However, interesting examples using a simple algebraic eddy-viscosity model can also be found in Sato et al. (1981), Kataoka and Serizawa (1995), Celik and Gel (2002), and Nikitopoulos and Michaelides (1995) for pipe flows, or Burns and Rice (1997) and Clark et al. (1990) for bubble columns and low liquid input bubbly flows.

In the present model, the Reynolds stress tensor $\tau_{\mathrm{Re}} = \langle \rho_k \vec{u}'_k \vec{u}'^t_k \rangle$ is approximated using an eddy-viscosity approach based on the bubbly flow algebraic model proposed by Sato et al. (1981). The total eddy viscosity is given by

$$\nu_t = \nu_{t_0} + \nu_{t_b} \tag{22}$$

where ν_{t_0} and ν_{t_b} are, respectively, the contribution of wall friction and bubble-induced turbulence. The wall-friction effects are modeled following Reichardt (1951) and including a wall-damping function $f(y^+)$ as proposed by van Driest (1956) for a realistic prediction in the near-wall region

$$\nu_{t_0} = \frac{KRu_L^*}{6}(1 - r^{*2})(1 + 2r^{*2})\, f(y^+) \tag{23}$$

in which $f(y^+) = (1 - e^{-y^+/A^+})^2$, $A^+ = 26$, $K = 0.41$, $y^+ = yu^*/\nu$, $r^* = r/R$, $u_L^* = \sqrt{\tau_w/\rho}$, and $\tau_w = (R/2)(\partial P/\partial z)_f$. The bubble-induced term is given by the model of Sato et al. (1981), also weighted by the wall-damping function suggested by van Driest (1956)

$$\nu_{t_b} = k_1 \varepsilon R_b |\vec{U}_g - \vec{U}_l| f(y^+) \tag{24}$$

with

$$k_1 = \begin{cases} k_{1,\max} & \text{if } r < R - R_b \\ -\dfrac{k_{1,\max}}{R_b - d_c} r - \dfrac{k_{1,\max}}{d_c - R_b}(R - d_c) & \text{if } R - R_b < r < R - d_c \\ 0 & \text{if } r > R - d_c \end{cases}$$

Because no bubbles are found very near to the wall (for $r > R - d_c$), the bubble-induced term is neglected in this part. The thickness of this layer is taken as $d_c = 20$ μm (Sato et al., 1981). The centerline value of k_1, given by $k_{1,\max}$, was found to be in the range of 1 to 1.4 by Sato et al. (1981). In some of our model results, the best agreement was found for lower values of $k_{1,\max}$. However, herein we will use the value of $k_{1,\max} = 1.2$ recommended by Sato et al. (1981), given that we want to develop a model free of input from individual experiments.

It should be noted that an additional contribution for taking into account the motion of the liquid around the bubbles can be added to this Reynolds stress formulation (Antal et al., 1991; Politano et al., 2003). In our model this term is neglected.

Final Formulation

Simplified set of equations

Following the formulation given in Eqs. 6 and 7 and the hypothesis, the system is explicitly written for the gas and the liquid phases. Using $\nu_t = \mu_t/\rho_l$ and $U_r = |\vec{U}_g - \vec{U}_l|$, and projecting on the r and z-axis lead to the following set of equations

$$\frac{\partial P_g}{\partial z} = \rho_g g - \frac{3}{8}\frac{1}{R_b} C_d \rho_l U_r^2 \tag{25}$$

$$\varepsilon \frac{\partial P_g}{\partial r} = -C_l \varepsilon \rho_l U_r \frac{\partial U_l}{\partial r} - \frac{\varepsilon \rho_l U_r^2}{R_b}\left[C_{w1} + C_{w2}\left(\frac{R_b}{R - r}\right)\right] - \frac{3}{8}\mu_t \frac{C_d}{R_b} U_r \frac{\partial \varepsilon}{\partial r} \tag{26}$$

$$(1 - \varepsilon)\frac{\partial P_l}{\partial z} = (1 - \varepsilon)\frac{1}{r}\frac{\partial}{\partial r}\left[r(\mu_l + \mu_t)\frac{\partial U_l}{\partial r}\right] + (1 - \varepsilon)\rho_l g + \frac{3}{8}\frac{\varepsilon}{R_b} C_d \rho_l U_r^2 \tag{27}$$

$$(1 - \varepsilon)\frac{\partial P_l}{\partial r} = C_p \rho_l U_r^2 (1 - \varepsilon)\frac{\partial \varepsilon}{\partial r} + C_l \varepsilon \rho_l U_r \frac{\partial U_l}{\partial r} + \frac{\varepsilon \rho_l U_r^2}{R_b}\left[C_{w1} + C_{w2}\left(\frac{R_b}{R - r}\right)\right] + \frac{3}{8}\mu_t \frac{C_d}{R_b} U_r \frac{\partial \varepsilon}{\partial r} \tag{28}$$

The gas phase velocity follows from $U_g(r) = U_l(r) + U_r$ in the present model. Equations 26–28 are combined to further simplify the numerical formulation. Using Eq. 21 for connecting the gas pressure to the liquid pressure, we obtain: $(1 - \varepsilon) \times$ Eq. 26 $- \varepsilon \times$ Eq. 28 $= \varepsilon(1 - \varepsilon)C_p \rho_l U_r^2 (\partial \varepsilon/\partial r)$. This relation will be used to derive Eq. 34.

Boundary conditions

The boundary conditions used are the following:

- No-slip condition for the liquid phase: $\vec{U}_l(r = R) = 0$
- The flow is axially symmetric: $(\partial U_l/\partial r)(r = 0) = 0$
- The area-averaged void fraction is specified: $\langle \varepsilon \rangle = c$
- The superficial liquid velocity value U_{sl} is specified and the pressure gradient $\partial P/\partial z$ is determined accordingly.

Numerical formulation

For convenience, the following variables are introduced: $a_l(r) = \partial U_l/\partial r$ and $\alpha(r) = 2\pi \int \varepsilon r dr$. Because we want to adjust the pressure gradient for a given liquid volumetric flux U_{sl} and area-averaged void fraction $\langle \varepsilon \rangle$, we also introduce $\gamma = \partial P/\partial z$ and the cumulative liquid flux $J_l(r) = (2/R^2) \int (1 - \varepsilon) U_l r dr$. The set of equations to solve is a system of six first-order differential equations, strongly coupled through the void fraction ε and liquid velocity U_l

$$\frac{\partial \gamma}{\partial r} = 0 \tag{29}$$

$$\frac{\partial J_l}{\partial r} = \frac{2}{R^2}(1-\varepsilon)U_l r \tag{30}$$

$$\frac{\partial \alpha}{\partial r} = 2\pi\varepsilon r \tag{31}$$

$$\frac{\partial U_l}{\partial r} = a_l(r) \tag{32}$$

$$\frac{\partial a_l}{\partial r} = \frac{\dfrac{\partial P}{\partial z} - \rho_l g}{\mu_l + \mu_t} - \left(\frac{1}{r} + \frac{1}{\mu_t + \mu_l}\frac{\partial \mu_t}{\partial r}\right)a_l - \frac{3C_d\rho_l U_r^2}{8R_b(\mu_l + \mu_t)}\frac{\varepsilon}{1-\varepsilon} \tag{33}$$

$$\frac{\partial \varepsilon}{\partial r} = \frac{-C_l\rho_l U_r a_l \varepsilon - \dfrac{\varepsilon\rho_l U_r^2}{R_b}\left(C_{w1} + C_{w2}\dfrac{R_b}{R-r}\right)}{\varepsilon(1-\varepsilon)C_{p_2}\rho_l U_r^2 + \dfrac{3}{8}\mu_t\dfrac{C_d}{R_b}U_r} \tag{34}$$

where $C_{p_2} = 2C_p = 1/2$ and U_r is evaluated from the mean void fraction $\langle\varepsilon\rangle$ by using the correlation of Garnier et al. (2002): $U_r = U_t(1 - \langle\varepsilon\rangle^{1/3})$. The terminal velocity U_t of a single bubble in an infinite medium is taken from the model of Peebles and Garber (1953). This expression for the bubble relative velocity was found to properly describe the changes of bubble relative velocity with mean void fraction for various experimental conditions (Guet et al., 2004).

In principle the bubble relative velocity can be computed by using the pressure gradient and the drag force correlation in the gas-phase axial momentum equation. Because in the present investigation we are especially interested in predicting the radial force effects by our simplified model, the simple relation suggested by Garnier et al. (2002) is used for the bubble relative velocity determination. This simplification avoids numerical instabilities arising from a coupling between the pressure gradient and the bubble relative velocity. However, we checked with our final results that the bubble relative velocity and pressure gradient values are consistent with the drag force model given by Ishii and Zuber (1979).

The quantities of input are: the area-averaged void fraction $\langle\varepsilon\rangle$, the superficial liquid velocity U_{sl}, and the bubble radius R_b. Reformulating the boundary conditions for our set of equations leads to the following:

- No-slip condition for the liquid phase: $\vec{U}_l(R) = 0$
- The flow is axially symmetric: $a_l(0) = 0$
- The area averaged void fraction specification: $\alpha(0) = 0$ and $\alpha(R) = \pi R^2\langle\varepsilon\rangle$
- To specify the liquid input, we impose $J_l(0) = 0$ and $J_l(R) = U_{sl}$

A set of six unknowns has to be determined by using six ordinary differential equations (ODEs) with six boundary conditions. The D02RAF NAG FORTRAN library was used, which is suitable for a full nonlinear problem. A deferred correction technique and Newton iterations were implemented. Because the lift force was a source of strong gradients, a continuation parameter was used to increase progressively the lift-force coefficient magnitude in an iterative loop. Typical computations consisted in 50 iterations on the lift force and used 10,000–50,000 mesh points. The numerical results are provided for a maximum norm corresponding to an error of $<5 \times 10^{-6}$ on the void fraction values.

Results and Discussion

Model validation

Comparison with Experiments from the Literature. To validate our simplified model, two sets of experimental data collected at differing liquid input and pipe diameter conditions are used:

(1) The experiment of Serizawa et al. (1975) in an air–water 60-mm-diameter pipe at $U_{sl} = 1.03$ m/s, $U_{sg} = 0.21$ m/s, $\langle\varepsilon\rangle = 0.18$, and $D_b = 4$ mm.

(2) The experiments of Liu and Bankoff (1993) in an air–water 38-mm-diameter pipe at $U_{sl} = 0.753$ m/s, $U_{sg} = 0.23$ m/s, $\langle\varepsilon\rangle = 0.19$, and $D_b = 3.6$ mm.

The results for the void fraction and radial profiles of liquid velocity obtained for these two experiments are shown in Figure 1. The model correctly describes the void fraction and liquid velocity for both pipe diameter values. The magnitude of the liquid velocity gradient at the wall is somehow underestimated (Figure 1b). To investigate the validity of our simplifications, the values of the superficial gas velocity are also compared. The superficial gas velocity, as obtained with our model calculations, was computed by applying $U_{sg} = (2/R^2)\int \varepsilon U \varepsilon r dr$, with $U_g = U_l + U_r$. The results are $U_{sg} = 0.196$ m/s and $U_{sg} = 0.212$ m/s for cases (1) and (2), respectively. These values are comparable to those reported by the authors ($U_{sg} = 0.21$ m/s and $U_{sg} = 0.23$ m/s). This confirms the validity of our bubble relative velocity formulation. However, in general, the superficial gas velocity was found to be slightly underpredicted by the model.

A better description of the liquid velocity profile was found by neglecting the bubble eddy-viscosity contribution, corresponding to $k_{1,\max} = 0$ in Eq. 24 (see Figure 2). This is consistent with the eddy-viscosity model developed in Chahed et al. (2003): the authors reported that the eddy viscosity in bubbly flow can be greater or smaller than the corresponding single-phase flow eddy viscosity, depending on a competition between bubble agitation (which tends to increase the eddy viscosity), and shear stress attenuation arising from turbulent isotropization by the bubbles (which decreases the appropriate eddy-viscosity value). Moreover, experimental investigations reported these turbulence damping effects (Serizawa and Kataoka, 1994). Because we want to capture the main trends with a simplified phenomenological model, however, we will use the initially proposed value of $k_{1,\max} = cste = 1.2$ by Sato et al. (1981) in our eddy viscosity formulation.

Moderate Liquid Input Predictions: Bubble Size Effects. We compared the radial profile results obtained with the model with experiments carried out in our pipe-flow experimental setup of 72-mm inner diameter. The comparison for $\mathrm{Re}_{sl} = 16{,}000$ and for two bubble size values are presented in Figure 3, corresponding to volumetric-spherical equivalent diameters of $D_b = 4$ and 8 mm. In the present experiments, the bubbles were ellipsoidal in shape, with a typical aspect ratio $\chi \approx 1.3$ and 1.9 for $D_b = 4$ and 8 mm, respectively (χ is the ratio of horizontal to vertical chord length of the bubbles). Our model

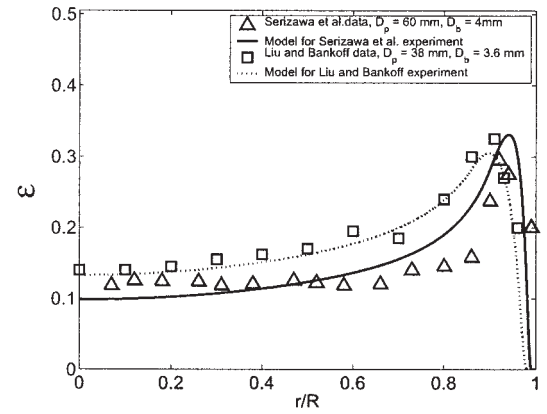

(a) Void fraction

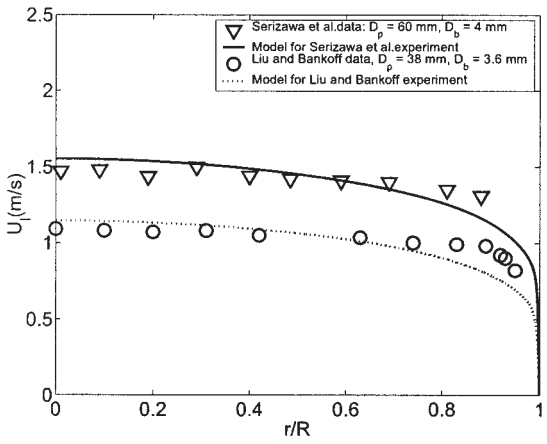

(b) Liquid velocity

Figure 1. Comparison between the experimental data of Serizawa et al. (1975) and Liu and Bankoff (1993) with the model results [with $k_1(r = 0) = 1.2$ in Eq. 24].

(a) Void fraction; (b) liquid velocity.

could not be applied to much larger bubbles: the simulations are restricted to $D_b < 10$ mm because larger bubbles are in the wobbling regime or spherical-cap shaped (Clift et al., 1978). The model is able to capture the wall- and core-peaking void fraction profiles associated with increased bubble diameter. Also, the liquid velocity evolution is well described by the model, changing from a flat to a parabolic profile with increasing bubble size. However, the profiles associated with the large bubble size experimental conditions are not as correctly predicted as the small bubble situation. This is attributed to the large distribution of bubble size during the large bubble experiments. Bubbles with a spherical equivalent diameter of <5 mm were also measured by our four-point probe near the wall location during this experiment. Therefore, to describe the profiles more closely, a model of multiple bubble-size classes, such as the one developed by Lucas et al. (2001) and Politano et al. (2003), would be needed. Also, a number of coefficients used in this model, such as C_p and C_d, might be changing with bubble size. However, our simplified model is found to properly capture the main effect of an increased bubble size on the radial profiles.

Bubble Column Predictions. We also computed the void fraction and liquid velocity field associated with various bubble size and void fraction conditions in an air–water bubble column, that is for $U_{sl} = 0$. In Figure 4 the void fraction and liquid velocity profiles obtained in a bubble column of diameter $D_p = 72$ mm for two bubble diameter values ($D_b = 4$ and 8 mm) and for an area-averaged void fraction $\langle\varepsilon\rangle = 0.05$ are presented. As observed in bubble column experiments, we obtain a liquid downflow at the wall (Clark et al., 1990; Mudde and Saito, 2001; Mudde et al., 1997). Although we use a turbulent pipe flow model for the eddy viscosity, as suggested by Sato et al. (1981), the liquid velocity profiles associated with bubble column conditions are qualitatively in agreement with experimental observations. Because of the change of sign of the lift-force coefficient when varying the bubble diameter, the void fraction profile is almost flat (with a small peak near the wall) for small bubbles, whereas a parabolic profile is obtained for large bubbles. The liquid recirculation is decreased when using small bubbles: the small bubbles are accumulating in the negative-velocity part of the flow, thus preventing the falling liquid flow by locally increasing the void fraction.

A near-wall peak of void fraction is found for small bubbles

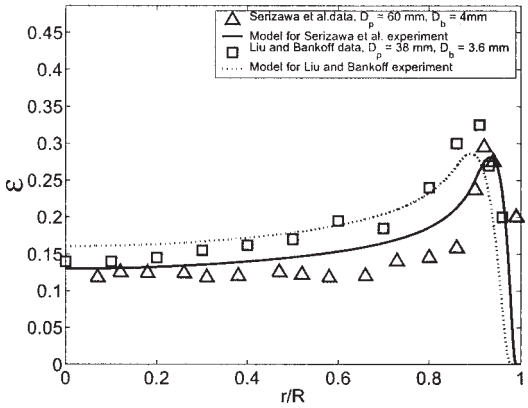

(a) Void fraction

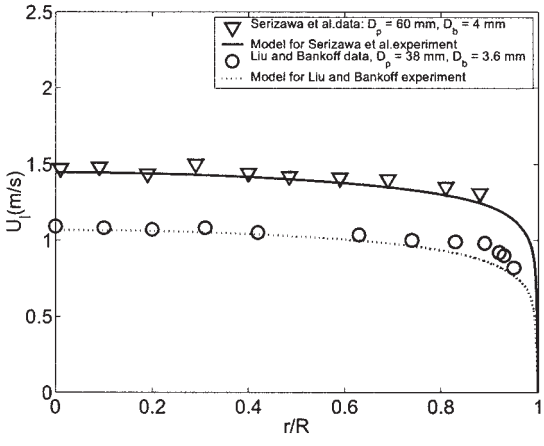

(b) Liquid velocity

Figure 2. Comparison between experimental data and model results when neglecting the bubble eddy viscosity (that is, using $k_1 = 0$ in Eq. 24).

(a) Void fraction; (b) liquid velocity.

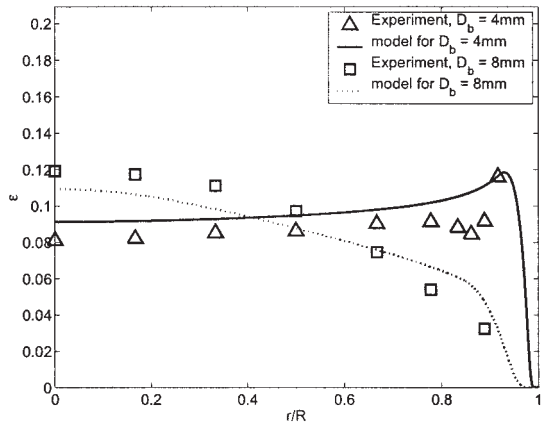

(a) Void fraction

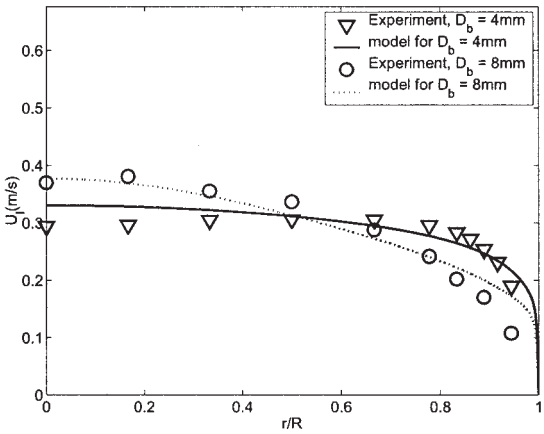

(b) Liquid velocity

Figure 3. Predictions obtained for our 72-mm inner diameter pipe flow, for Re_{sl} = 16,000, and for D_b = 4 and 8 mm.

(a) Void fraction; (b) liquid velocity. The model results are compared with experiments corresponding to $D_b = 4$ mm and $D_b \approx 8$ mm.

because, in that case, there is a competition between the radial forces. This peak is located at the pipe radial position corresponding to $\vec{F}_{g,lift} + \vec{F}_{g,wall} = 0$ (see Eq. 34). For the bubble column *case* with $D_b = 4$ mm, it is found at $r/R \approx 0.94$ (Figures 4 and 5a). For the large bubble case ($D_b = 8$ mm), both the lift and the wall force are negative, and thus no wall peak of void fraction is obtained (Figures 4 and 5b).

If the column diameter is increased it can be expected that the thickness of the inversed velocity gradient layer near the wall will be increased. This can lead to important inversed lift-force effects, resulting in a core peaking void fraction radial profile in large-diameter columns, even when using small bubbles with a positive lift-force coefficient. In the present simulations, the lift force was negligible in the inversed liquid vorticity layer because of the low value of the pipe diameter. In the case of large-diameter bubble columns the wall peaking of void fraction is in general not reported in the literature, even when the bubble size is low (Mudde and Saito, 2001). However, devoted bubble column experiments have shown that, provided a special attention was paid to the bubble injector, a peak of void fraction in the wall region could be found when the bubbles were small (Harteveld et al., 2003).

These results suggest that other mechanisms play an important role in the radial distribution phenomena in bubble columns, such as coherent structures and pipe diameter effects. More research is thus needed for a proper modeling of bubble column flow conditions by a simplified Euler–Euler approach. In the present study we are interested in flows with a net liquid input value, and thus this bubble column flow situation is seen as a limiting case for our simulations.

Low Liquid Input Predictions. We also compare our simulations with experimental results collected at low Re_{sl} conditions. In those conditions, a liquid downflow at the wall was also found. Similar measurement results for low liquid input flow conditions are reported in Mudde and Saito (2001). In Figure 6, we compare the void fraction and velocity measurements with model predictions for $Re_{sl} = 1200$; $D_b = 6.5$ mm, and a low area-averaged void fraction $\langle \varepsilon \rangle = 0.01$. In those conditions, the profiles of void fraction and liquid velocity were properly predicted with our model. At increased void fraction, however, the liquid recirculation was systematically

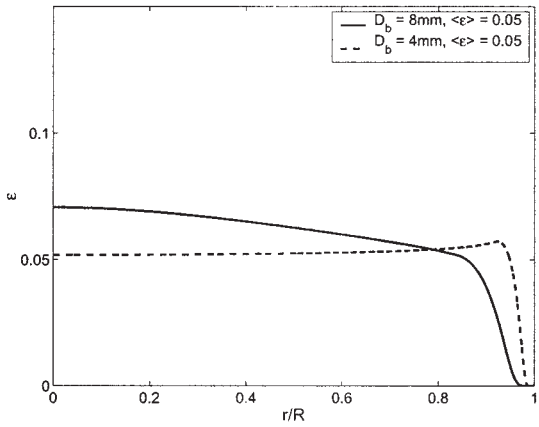

(a) Void fraction

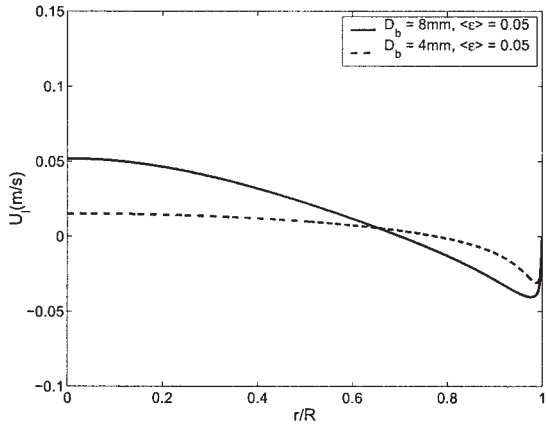

(b) Liquid velocity

Figure 4. Typical void fraction and velocity radial profiles in the bubble column mode as predicted by the model for D_b = 4 and 8 mm.

The mean void fraction is $\langle \varepsilon \rangle = 0.05$ and the pipe diameter $D_p = 72$ mm.

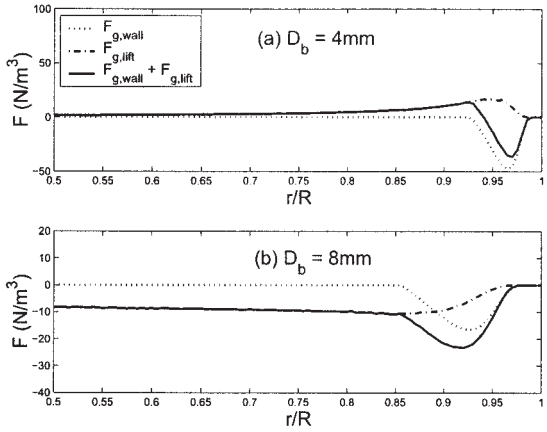

Figure 5. Radial wall and lift force predicted by the model in the bubble column-flow mode.

(a) $D_b = 4$ mm, $\langle\varepsilon\rangle = 0.05$; (b) $D_b = 8$ mm, $\langle\varepsilon\rangle = 0.05$. In case (a), there is a competition between the lift and wall force. The near-wall void fraction peak is obtained where $F_{g,wall} + F_{g,lift} = 0$.

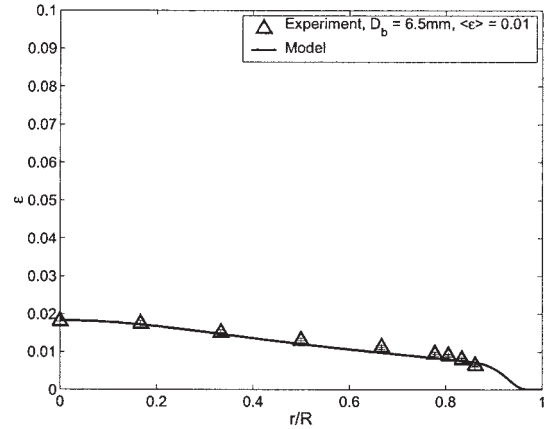

(a) Void fraction

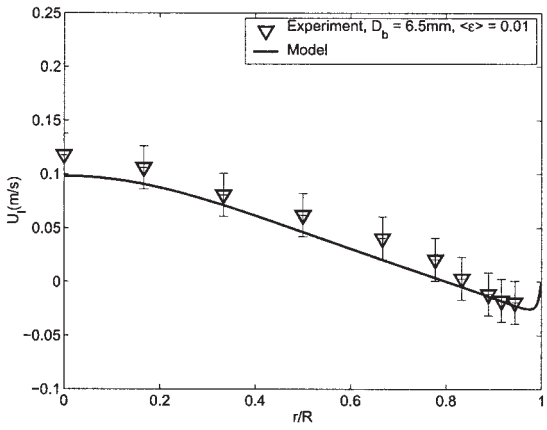

(b) Liquid velocity

Figure 6. Comparison of the velocity profiles obtained from the model and the experiments at Re_{sl} = 1200, $\langle\varepsilon\rangle$ = 0.01, and D_b = 6.5 mm.

(a) Void fraction; (b) liquid velocity.

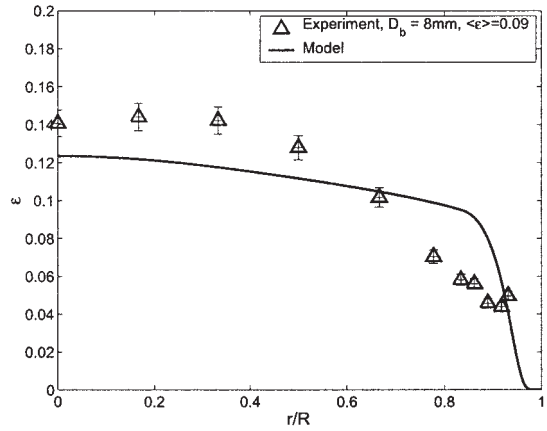

(a) Void fraction

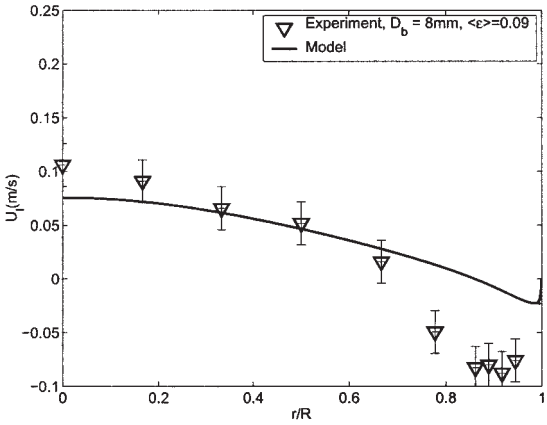

(b) Liquid velocity

Figure 7. Comparison of the void fraction and velocity radial profiles obtained from the model and the experiments at Re_{sl} = 1200, $\langle\varepsilon\rangle$ = 0.09, and D_b = 8 mm.

(a) Void fraction; (b) liquid velocity. In that case the liquid recirculation is underpredicted by the model.

underpredicted by our model, independently from the bubble size conditions (see Figure 7 for $Re_{sl} = 1200$, $D_b = 8$ mm, and $\langle\varepsilon\rangle = 0.09$). This can be due to a number of effects, such as the polydisperse aspects of the medium attributed to bubble fragmentation, bubble entrainment in the downflow regions, and bubble coalescence. Also, our pipe flow eddy-viscosity model is clearly not appropriate for low liquid input flows, for which the pipe Reynolds number is below the critical value corresponding to the transition to turbulence. In those conditions our simplified approach is therefore of limited interest. For our drift-flux distribution parameter calculations, we will restrict our computations to turbulent pipe flow conditions (we will use $Re_{sl} = 2000$ as a lower limit for U_{sl}).

Drift-flux distribution parameter

In this section we use our model for making predictions of the change of the distribution parameter with liquid input and bubble size in our 72-mm-diameter pipe flow. For that purpose, we carry out series of simulations at varied U_{sl} and R_b values. The distribution parameter, defined by Eq. 3 in the drift-flux

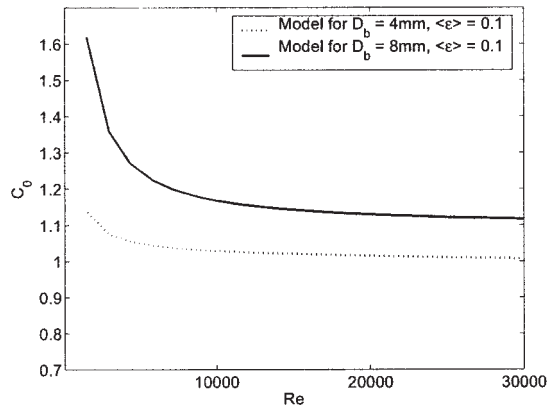

(a) Model

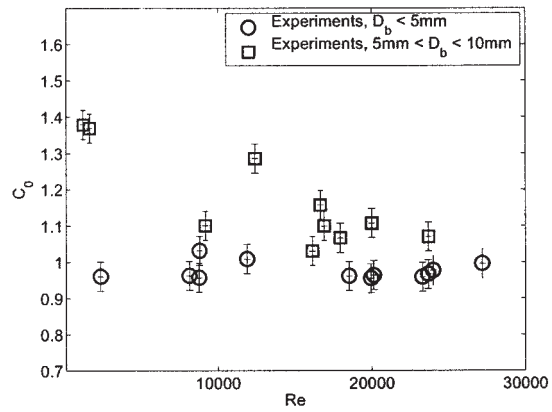

(b) Experiments

Figure 8. Distribution parameter as a function of the liquid input Reynolds number.

(a) Model results for $D_b = 4$ and 8 mm with $\langle\varepsilon\rangle = 0.1$; (b) experimental results at various area average void fraction conditions. The experiments are separated in wall peaking ($D_b < 5$ mm) and core-peaking void fraction radial profile conditions ($D_b > 5$ mm).

model (Zuber and Findlay, 1965), is calculated for each simulation by using the computed profiles. The experimental distribution parameter C_0 was also computed by applying Eq. 3 to the measured profiles of void fraction and phase velocities (Guet et al., 2004).

Liquid Input. We computed the effect of the liquid input for two different values of the bubble size corresponding to $D_b = 4$ and 8 mm, as shown in Figure 8a. The area-averaged void fraction was kept constant at $\langle\varepsilon\rangle = 0.1$ in those calculations. A few simulations were carried out at varied void fraction conditions. No substantial changes were found. In general we observed a significant increase of the C_0 parameter at decreased liquid input, as a result of the appearance of liquid recirculation in the near-wall region. It is interesting to note that reducing the bubble size reduces the C_0 parameter at any liquid input conditions. This is also observed in the experiments: the liquid recirculation was prevented by the small bubbles, thus reducing C_0. In Figure 8b we also plot our experimental data collected for different bubble size conditions, corresponding to the wall peaking of void fraction ($D_b < 5$ mm) and to the core peaking radial profile of void fraction ($D_b > 5$ mm) (Guet et al., 2004). The numerical simulation and experiments describe the same behavior at low liquid input for large bubbles: the C_0 parameter increases significantly when reducing the liquid input below $\mathrm{Re}_{sl} < 10{,}000$. Each C_0 experimental point is computed according to measured void fraction and velocity profiles. During these experiments, the void fraction has been varied from $\langle\varepsilon\rangle = 0.02$ to $\langle\varepsilon\rangle = 0.2$. This explains the scatter in the experimental data. From this plot, however, it is clear that the bubble size is a critical parameter for a proper description of the flow and accurate pressure drop predictions, as a result of the associated changes of the lift force.

Bubble Size. We also computed the C_0 parameter for various bubble size values when operating at a fixed large liquid input, for which no liquid downflow at the wall was obtained. These conditions were taken as $U_{sl} = 1.39$ m/s, that is, $\mathrm{Re}_{sl} = 100{,}000$ for the simulations. The area-averaged void fraction was fixed at $\langle\varepsilon\rangle = 0.1$. The results of the simulations are shown in Figure 9a.

In Figure 9b we also show experimental data collected in our experimental setup at moderate to large liquid input conditions. During these measurements, no liquid downflow was observed at the wall. This corresponds to $\mathrm{Re}_{sl} > 20{,}000$. The numerical

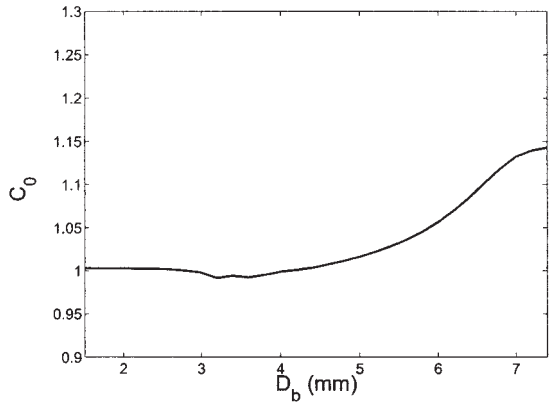

(a) Model

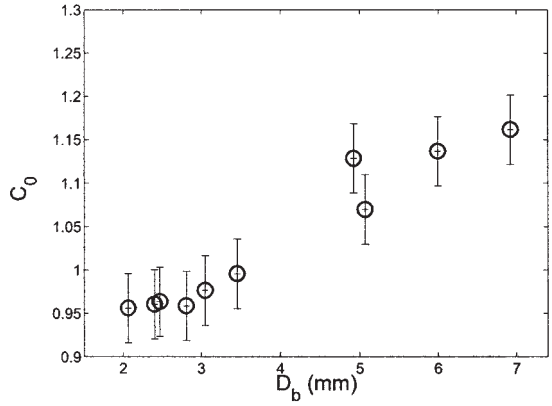

(b) Experiments

Figure 9. Distribution parameter as a function of the spherical-equivalent bubble diameter.

(a) Simulation results for $\mathrm{Re}_{sl} = 100{,}000$, $D_p = 72$ mm, and $\langle\varepsilon\rangle = 0.1$; (b) collected experiments for $D_p = 72$ mm, $\mathrm{Re}_{sl} > 20{,}000$, and various area average void fraction.

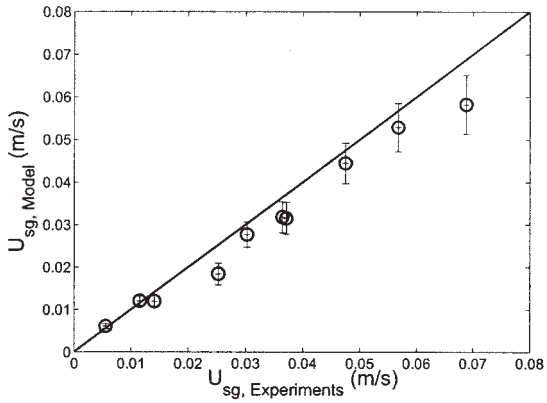

Figure 10. Comparison between the superficial gas velocity taken from the experiments and the model predictions.

For each simulation the area average void fraction and mean bubble diameter are taken from the corresponding measurement.

results show the same behavior as in the experiments: because of the lift force changes with bubble size, the C_0 parameter changes dramatically near $D_b = D_{b,neutral}$ ($D_{b,neutral}$ is the bubble diameter associated with a "neutral " lift force, that is, $C_l = 0$: $D_{b,neutral} = 5.8$ mm for water). Small bubbles ($D_b < D_{b,neutral}$) lead to $C_0 \approx 0.9$–1, whereas larger bubbles ($D_b > D_{b,neutral}$) give $C_0 \approx 1.1$–1.2, although there is a shift between the experimental and numerical results. This is attributed to the differences of liquid input and of void fraction conditions during the experiments and for the simulations, as well as the method of evaluation of the spherical-equivalent bubble size during the experiments, which was based on the correlation of Wellek et al. (1966) for connecting the volumetric spherical equivalent diameter to the measured bubble vertical chord length. In the next section, we will compare the superficial gas velocity values as obtained with our model with these measurements.

Superficial Gas Velocity. Under practical laboratory and gas-lift conditions, the input gas flow rate is often known, rather than the area-averaged void fraction. Our model would therefore have to be used in an iterative way for predicting the pressure drop associated with a given gas input. We thus investigate in this section whether our model can be used to predict the superficial gas velocity associated with given void fraction and bubble size conditions. We compared our predicted superficial gas velocity values with experimental data collected for various bubble diameter and void fraction conditions. In those simulations, the liquid input, area-averaged void fraction, and mean spherical-equivalent bubble diameter were taken from the measurements. The superficial gas velocities as measured by area-averaging our gas flux measurements (using the four-point optical-fiber probe technique) are compared with the associated model predictions in Figure 10. The comparisons are reasonable with respect to the accuracy of the measurement technique and the simplicity of our model. At large gas input, the model had the tendency to underpredict the superficial gas velocity. These increased gas input points correspond to increased void fraction ($\varepsilon > 0.1$), suggesting that the validity of our approach is restricted in terms of void fraction conditions. Improvements are expected if we would consider the local changes of the bubble relative velocity with local void fraction. However, as illustrated previously this effect has only a minor impact on the C_0 parameter determination.

Conclusion

In this contribution a simplified model, based on the two-fluid Euler–Euler modeling approach, has been developed for predicting the void fraction and velocity radial profiles at given bubble size and liquid input conditions. This model is able to capture the main trends associated with bubble size and liquid input changes. The most important phenomena are: (1) the transition from wall peaking to core peaking of void fraction for increased bubble diameter, and (2) the liquid downflow at the wall for low liquid input conditions.

Our two-fluid model used the lift force coefficient correlation as proposed by Tomiyama et al. (2002) for taking into account the bubble shape effects. This force term was found to be crucial for properly describing the changes of void fraction radial profiles with increased bubble size. This also had an impact on the liquid velocity profiles. At low liquid input, the liquid downflow at the wall was enhanced when increasing the bubble size because of an increased mixture density in the downflow region. This effect was also observed in the experiments.

From the void fraction and velocity profiles obtained at various flow conditions, we computed the drift-flux distribution parameter C_0 as defined in Zuber and Findlay (1965). A reasonable description of the distribution parameter as a function of bubble size and liquid input was achieved. Typical values were $C_0 \approx 1$ for small bubbles at large liquid input, and up to $C_0 \approx 1.5$ for large bubbles at low liquid input. The present model could be further improved by using an eddy-viscosity model able to predict turbulence damping, such as the one suggested by Chahed et al. (2003), and by taking into account the bubble velocity fluctuations and the associated effects on the interfacial forces, as suggested in Lathouwers (1999) and Chahed et al. (2003). Such an additional contribution could be included by using the approach described in Mudde and Simonin (1999). With these additional models the prediction of bubble column flows in large-diameter pipes ($D_p > 10$ cm) could be investigated in more detail. For a proper upscaling of gas-lift conditions as encountered during the application, it would also be interesting to extend the present model to larger pressure conditions.

Literature Cited

Antal, S. P., R. T. Lahey, and J. E. Flaherty, "Analysis of Phase Distribution in Fully Developed Laminar Bubbly Two Phase Flow," *Int. J. Multiphase Flow*, **7**, 635 (1991).

Burns, L. F., and R. G. Rice, "Circulation in Bubble Columns," *AIChE J.*, **43**, 1390 (1997).

Carrica, P. M., D. Drew, F. Bonetto, and R. T. Lahey, "A Polydisperse Model for Bubbly Two-Phase Flow around a Surface Ship," *Int. J. Multiphase Flow*, **25**, 257 (1999).

Celik, I., and A. Gel, "A New Approach in Modeling Phase Distribution in Fully Developed Bubbly Pipe Flow," *Flow Turbulence Combust.*, **68**, 289 (2002).

Chahed, J., and L. Masbernat, "Effet de parois sur la distribution de taux de vide dans les ecoulements a bulles," *C. R. Acad. Sci.*, **326**(2b), 719 (1998).

Chahed, J., V. Roig, and L. Masbernat, "Eulerian–Eulerian Two-Fluid Model for Turbulent Gas–Liquid Bubbly Flows," *Int. J. Multiphase Flow*, **29**, 23 (2003).
Clark, N. N., J. W. Van Egmond, and E. P. Nebiolo, "The Drift-Flux Model Applied to Bubble Columns and Low Velocity Flows," *Int. J. Multiphase Flow*, **16**, 261 (1990).
Clift, R., J. R. Grace, and M. E. Weber, *Bubbles, Drops and Particles.* Academic Press, New York (1978).
Drew, D. A., "A Turbulent Dispersion Model for Particles or Bubbles," *J. Eng. Math.*, **41**, 259 (2001).
Drew, D. A., and R. T. Lahey, "Phase Distribution Mechanisms in Turbulent Low-Quality Two-Phase Flow in a Circular Pipe," *J. Fluid Mech.*, **117**, 91 (1982).
Garnier, C., M. Lance, and J. L. Marie, "Measurement of Local Flow Characteristics in Buoyancy-Driven Bubbly Flow at High Void Fraction," *Exp. Therm. Fluid Sci.*, **26**, 811 (2002).
Guet, S., R. V. Fortunati, R. F. Mudde, and G. Ooms, "Bubble Velocity and Size Measurements with a Four-Point Optical Fiber Probe," *Part. Part. Syst. Char.*, **20**, 219 (2003b).
Guet, S., G. Ooms, R. V. A. Oliemans, and R. F. Mudde, "Bubble Injector Effect on the Gaslift Efficiency," *AIChE J.*, **49**, 2242 (2003a).
Guet, S., G. Ooms, R. V. A. Oliemans, and R. F. Mudde, "Bubble Size Effect on Low Liquid Input Drift-Flux Parameters," *Chem. Eng. Sci.*, **59**, 3315 (2004).
Guet, S., H. R. E. Van Maanen, and R. F. Mudde, "Feasibility of LDA Measurement in High Void Fraction Bubbly Flow," Proc. of the 11th Symp. on Application of Laser Technique to Fluid Mechanics, Lisbon, Portugal (2002).
Harteveld, W. K., R. F. Mudde, and H. E. A. Van den Akker, "Dynamics of a Bubble Column: influence of Gas Distribution on Coherent Structures," *Can. J. Chem. Eng.*, **81**, 389 (2003).
Hill, D. P., D. M. Wang, A. D. Gosman, and H. I. Issa, "Numerical Prediction of Two-Phase Bubbly Flow in a Pipe," Proc. of 2nd Int. Conf. on Multiphase Flow, Kyoto, Japan (1995).
Ishii, M., *Thermo-Fluid Dynamic Theory of Two-Phase Flow.* Eyrolles, Paris (1975).
Ishii, M., and N. Zuber, "Drag Coefficient and Relative Velocity in Bubbly, Droplet, or Particulate Flows," *AIChE J.*, **25**, 843 (1979).
Kataoka, I., and A. Serizawa, "Modeling and Prediction of Turbulence in Bubbly Two-Phase Flow," Proc. of 2nd Int. Conf. on Multiphase Flow, Kyoto, Japan (1995).
Lance, M., and M. Lopez de Bertodano, "Phase Distribution Phenomena and Wall Effects in Bubbly Two-Phase Flow," *Multiphase Sci. Technol.*, **8**, 69 (1994).
Lathouwers, D., *Modelling and Turbulent Simulation of Turbulent Bubbly Flow.* PhD Thesis, Delft, The Netherlands: Delft University of Technology (1999).
Liu, T. J., and S. G. Bankoff, "Structure of Air–Water Bubbly Flow in a Vertical Pipe. 2: Void Fraction, Bubble Velocity and Bubble Size Distribution," *J. Heat Transfer*, **36**, 1061 (1993).
Lopez de Bertodano, M., R. T. Lahey, and O. C. Jones, "Phase Distribution in Bubbly Two-Phase Flow in Vertical Ducts," *Int. J. Multiphase Flow*, **20**, 805 (1994).
Lucas, D., E. Krepper, and H. M. Prasser, "Prediction of Radial Gas Profiles in Vertical Pipe Flow on the Basis of Bubble Size Distribution," *Int. J. Therm. Sci.*, **40**, 217 (2001).
Moraga, F. J., D. A. Drew, and R. T. Lahey, "The Modeling of Wall-Induced Forces in Two-Fluid Model Simulations of a Bubbly Flow," Proc. of the 5th Int. Conf. on Multiphase Flow, Yokohama, Japan (2004).
Moraga, F. J., A. E. Larreteguy, D. A. Drew, and R. T. Lahey, Jr., "Assessment of Turbulent Dispersion Models for Bubbly Flows in the Low Stokes Number Limit," *Int. J. Multiphase Flow*, **29**, 655 (2003).
Mudde, R. F., J. S. Groen, and H. E. A. Van den Akker, "Liquid Velocity Field in a Bubble Column: LDA Experiments," *Chem. Eng. Sci.*, **52**, 4217 (1997).
Mudde, R. F., and T. Saito, "Hydrodynamical Similarities between Bubble Column and Bubbly Pipe Flow," *J. Fluid Mech.*, **437**, 203 (2001).
Mudde, R. F., and O. Simonin, "Two and Three-Dimensional Simulations of a Bubble Plume Using a Two-Fluid Model," *Chem. Eng. Sci.*, **54**, 5061 (1999).
Nikitopoulos, D. E., and E. E. Michaelides, "Phenomenological Model for Dispersed Bubbly Flow in Pipes," *AIChE J.*, **1**, 12 (1995).
Peebles, F. N., and H. J. Garber, "Studies on the Motion of Gas Bubbles in Liquids, " *Chem. Eng. Prog.*, **49**, 88 (1953).
Politano, M. S., P. M. Carrica, and J. Converti, "A Model for Turbulent Polydisperse-Two Phase Flow in Vertical Channels," *Int. J. Multiphase Flow*, **29**, 1153 (2003).
Reichardt, H., "Vollstandige Darstellung der turbulenten Geschwindigkeittsverteilung in glatten Leitungen," *ZAMM*, **31**, 208 (1951).
Sato, Y., L. Sadatomi, and K. Sekogushi, "Momentum and Heat Transfer in Two Phase Bubbly Flow," *Int. J. Multiphase Flow*, **7**, 167 (1981).
Serizawa, A., and I. Kataoka, "Dispersed Flow—I," *Multiphase Sci. Technol.*, (1994)8, 125 .
Serizawa, A., I. Kataoka, and I. Michiyoshi, "Turbulence Structure of Air–Water Bubbly Flows—2. Local Properties," *Int. J. Multiphase Flow*, **2**, 235 (1975).
Stuhmiller, J. H., "The Influence of Interfacial Pressure Forces on the Character of Two-Phase Flow Model Equations," *Int. J. Multiphase Flow*, **3**, 551 (1977).
Tomiyama, A., "Struggle with Computational Bubble Dynamics," Proc of 3rd Int. Conf. on Multiphase Flow, Lyon, France (1998).
Tomiyama, A., H. Tarnai, I. Zun, and S. Hosokawa, "Transverse Migration of Single Bubbles in Simple Shear Flow," *Chem. Eng. Sci*., **57**, 1849 (2002).
Troshko, A. A., and Y. A. Hassan, "A Two-Equation Turbulence Model of Turbulent Bubbly Flow," *Int. J. Multiphase Flow*, **27**, 1965 (2002).
van Driest, E. R., "On Turbulent Flow Near a Wall," *J. Aeron. Sci.*, **23**, 1007 (1956).
Wellek, R. M., A. K. Arawal, and A. H. P. Skelland, "Shapes of Liquid Drops Moving in Liquid Media," *AIChE J.*, **12**, 854 (1966).
Zuber, N., and J. A. Findlay, "Average Volumetric Concentration in Two-Phase Flow Systems," *J. Heat Transfer Trans. ASME*, **87**, 453 (1965).

Manuscript received Jan. 21, 2004, and revision received Oct. 26, 2004.